
Immuno-PET and Immuno-SPECT of Rheumatoid Arthritis with Radiolabeled Anti-Fibroblast Activation Protein Antibody Correlates with Severity of Arthritis

Peter Laverman¹, Tessa van der Geest¹, Samantha Y.A. Terry^{1,2}, Danny Gerrits¹, Birgitte Walgreen³, Monique M. Helsen³, Tapan K. Nayak⁴, Anne Freimoser-Grundschober⁵, Inja Waldhauer⁵, Ralf J. Hosse⁵, Ekkehard Moessner⁵, Pablo Umana⁵, Christian Klein⁵, Wim J.G. Oyen¹, Marije I. Koenders³, and Otto C. Boerman¹

¹Department of Radiology and Nuclear Medicine, Radboud University Medical Center, Nijmegen, The Netherlands; ²Department of Imaging Chemistry and Biology, King's College London, London, United Kingdom; ³Department of Experimental Rheumatology, Radboud University Medical Center, Nijmegen, The Netherlands; ⁴Roche Pharmaceutical Research and Early Development, Innovation Center Basel, Basel, Switzerland; and ⁵Roche Pharmaceutical Research and Early Development, Innovation Center Zurich, Schlieren, Switzerland

One of the most prominent cell populations playing a role in rheumatoid arthritis (RA) is activated fibroblast-like synoviocytes. Among many other proteins, fibroblast-like synoviocytes dominantly express fibroblast activation protein (FAP). Because of the high expression of FAP in arthritic joints, radioimmunoimaging of activated fibroblasts with anti-FAP antibodies might be an attractive noninvasive imaging tool in RA. **Methods:** SPECT and PET with ¹¹¹In- and ⁸⁹Zr-labeled anti-FAP antibody 28H1 was performed in mice with CIA. The radioactivity uptake in joints was quantified and correlated with arthritis score. **Results:** Both ¹¹¹In-28H1 and ⁸⁹Zr-28H1 showed high uptake in inflamed joints, being 3-fold higher than that of the irrelevant isotype-matched control antibody DP47GS, clearly indicating specific accumulation of 28H1. Uptake of ¹¹¹In-28H1 ranged from 2.2 percentage injected dose per gram (%ID/g) in noninflamed joints to 32.1 %ID/g in severely inflamed joints. DP47GS accumulation ranged from 1.6 %ID/g in noninflamed tissue to 12.0 %ID/g in severely inflamed joints. Uptake of 28H1 in inflamed joints correlated with arthritis score (Spearman ρ , 0.69; $P < 0.0001$) and increased with severity of arthritis. **Conclusion:** SPECT/CT imaging with the anti-FAP antibody ¹¹¹In-28H1 specifically visualized arthritic joints with high resolution, and tracer accumulation correlated with the severity of the inflammation in murine experimental arthritis. Background uptake of the radiolabeled antibody was low, resulting in excellent image quality. ⁸⁹Zr-28H1 was less favorable for RA imaging because of an elevated bone uptake of ⁸⁹Zr. Future studies will focus on the potential role of 28H1 as a tool to monitor therapy response early on.

Key Words: fibroblast activation protein (FAP); SPECT imaging; PET imaging; CIA; monoclonal antibody

J Nucl Med 2015; 56:778–783

DOI: 10.2967/jnumed.114.152959

Rheumatoid arthritis (RA) is an autoimmune disease that results in chronic and systemic inflammation in synovial joints. RA is characterized by hyperplasia and chronic inflammation of synovial membranes that invade into articular cartilage and bone. Many cell types that play a role in joint destruction are present in the synovial lining layer. One of the most prominent cell populations is activated fibroblast-like synoviocytes, which are involved in pannus formation (1). Among many other proteins, fibroblast-like synoviocytes dominantly express fibroblast activation protein (FAP) (2). It has previously been shown that the area in which these FAP-expressing fibroblast-like synoviocytes are present corresponds with the center of high inflammatory activity (2).

FAP is a cell surface-bound, type II transmembrane glycoprotein belonging to the family of serine prolyl oligopeptidases, has a molecular weight of 95 kDa, and is abundantly expressed in granulation tissue of healing wounds (3,4). It has been shown that FAP is closely related to dipeptidylpeptidase IV, also known as CD26 (5). Besides peptidase activity, it was demonstrated that FAP has collagenase activity in vitro (6). FAP is also found in more than 90% of human epithelial carcinomas (3,7), in which its expression is limited to fibroblasts in the tumor stroma (8). We hypothesized that, because of high expression of FAP in arthritic joints, radioimmunoimaging of activated fibroblasts with anti-FAP antibodies might be an attractive noninvasive imaging tool in RA.

Because FAP is expressed in tumor stroma, various anti-FAP antibodies have been studied for radioimmunotargeting of malignancies. Among these are ¹³¹I-labeled murine F19 (9) and ¹³¹I-labeled sibrotuzumab, a humanized version of the F19 antibody (10). More recently, 2 new anti-FAP antibodies, ESC11 and ESC14, were labeled with ¹⁷⁷Lu, which showed excellent targeting in melanoma xenografts (11).

In the present study, we investigated the potential of a radiolabeled anti-FAP antibody for specific PET and SPECT of activated fibroblasts in an experimental model of RA. Although PET is generally better for quantification purposes, preclinical SPECT imaging has a higher resolution.

Fischer et al. grafted the human anti-FAP Fab fragments into the human IgG1 framework, resulting in fully human anti-FAP IgG1 antibodies (11). Here we used the 28H1 antibody, which is

Received Dec. 10, 2014; revision accepted Mar. 17, 2015.
For correspondence or reprints contact: Peter Laverman, Radboud University Medical Center, Department of Radiology and Nuclear Medicine, P.O. Box 9101, 6500 HB Nijmegen, The Netherlands.
E-mail: peter.laverman@radboudumc.nl
Published online Apr. 9, 2015.
COPYRIGHT © 2015 by the Society of Nuclear Medicine and Molecular Imaging, Inc.

a noninternalizing anti-FAP antibody with high picomolar affinity for both murine and human FAP and bearing mutations in the Fc part, preventing binding to the Fc γ receptors. In brief, the antibody was conjugated with desferal for ^{89}Zr labeling and with diethylenetriaminepentaacetic acid (DTPA) to allow ^{111}In labeling. PET/CT and SPECT/CT imaging studies and biodistribution studies were performed in mice with collagen-II-induced arthritis (CIA) to correlate the radioactivity concentration in the joints with the severity of arthritis.

MATERIALS AND METHODS

Animals

Male DBA/1J mice were obtained from Janvier-Elevage. All mice were housed in filter-top cages under specific pathogen-free conditions, and a standard diet and water were provided ad libitum. The mice were used between 10 and 12 wk of age. All animal procedures were approved by the institutional animal welfare committee and performed according to their guidelines.

Antibody Conjugation and Radiolabeling

The monoclonal anti-FAP antibody 28H1 has high avidity for murine (<1 pM) and human FAP (268 pM) and has the P329G LALA mutations in the Fc part to make it Fc effector silent. The monoclonal antibody DP47GS with the P329G LALA mutations served as an isotype-matched control antibody with no known binding specificity and no affinity for murine or human FAP. The 28H1 anti-FAP antibody is a fully human FAP antibody that was generated by phage display using recombinant FAP (12). To abolish Fc γ R and C1q binding, a P329G LALA mutation was introduced that completely abolished Fc γ R and C1q binding but did not affect FcRn binding and pharmacokinetics (13).

Both 28H1 and DP47GS were conjugated with isothiocyanatobenzyl-diethylenetriaminepentaacetic acid (p-SCN-Bz-DTPA) (Macrocyclics, Inc.) according to standard procedures. Labeling with $^{111}\text{InCl}_3$ (Mallinckrodt BV) was performed as described previously (14). Labeling efficiencies were greater than 99% and 89% for ^{111}In -DTPA-28H1 and ^{111}In -DTPA-DP47GS, respectively. ^{111}In -DTPA-DP47GS was purified on a PD-10 column (GE Healthcare Biosciences) and eluted with phosphate-buffered saline (PBS), containing 0.5% bovine serum albumin, to provide 2 preparations with a radiochemical purity of 99% or greater.

In addition, the 28H1 antibody was modified with succinyl-desferal-iron-tetrafluorophenol ester (VU University Medical Center) as described previously (15). The 28H1-desferal conjugate (1 mg) was radiolabeled with 110 MBq of ^{89}Zr (PerkinElmer) in 0.5 M *N*-(2-hydroxyethyl)piperazine-*N'*-(2-ethanesulfonic acid), pH 7.2, for 60 min at 37°C. Labeling efficiency was 97% as determined by instant thin-layer chromatography. The reaction mixture was purified on a PD-10 column eluted with gentisic acid (5 mg/mL). The radiochemical purity of ^{89}Zr -*N*-succinyl-desferal-28H1 (^{89}Zr -28H1) was greater than 99%.

^{18}F -FDG was purchased as a ready-to-use product (GE Healthcare).

Binding Assay of 28H1

The human fibroblast cell line GM05389 and murine 3T3 fibroblasts stably transfected with murine FAP were detached with cell dissociation buffer and resuspended in fluorescence-activated cell sorting (FACS) buffer. Cells (200,000) were seeded into a 96-well round bottom plate. The plate was centrifuged at 400g for 3 min to pellet the cells. The supernatant was removed, and cells were resuspended in 40 μL of Alexa647-labeled anti-FAP 28H1 or DP47GS at 10 $\mu\text{g}/\text{mL}$. The plate was incubated for 30 min at 4°C to allow binding of the antibodies. To remove unbound antibodies, the cells were centrifuged again, washed twice with FACS buffer, and resuspended in 200 μL of FACS buffer, and the fluorescence was measured by flow cytometry.

Animal Experiments

For the induction of CIA, Freund complete adjuvant and *Mycobacterium tuberculosis* (strain H37Ra) were obtained from Difco. Bovine collagen type II (CII) was prepared as described previously (16). DBA/1J mice were immunized intradermally at the base of the tail with 100 μg of CII. Three weeks later, mice received an intraperitoneal booster injection of 100 μg of CII dissolved in PBS. The onset of arthritis occurred a few days after the booster injection. Clinical onset and progression was monitored by macroscopic scoring of the paws, on a scale of 0 to 2 for each paw, in a masked fashion by 2 independent observers. Cumulative scoring based on redness, swelling, and, in later stages, ankylosis was as follows: 0, no changes; 0.25, 1–2 toes red or swollen; 0.5, 3–5 toes red or swollen; 1, swollen ankle; 1.5, swollen footpad; 2, severe swelling and ankylosis. Naïve mice—that is, not immunized—were used as controls. Mice were injected with the radiolabeled antibodies at day 24–26 after start of the immunization. SPECT/CT imaging with ^{111}In -28H1 and ^{111}In -DP47GS was performed as follows. Mice ($n = 3/\text{group}$) received an intravenous injection of 15–18 MBq of ^{111}In -28H1 or ^{111}In -DP47GS (injected dose, 50 μg). At 1 and 3 d after injection, images were acquired with the U-SPECT-II/CT (MILabs) (17). Mice were scanned under general anesthesia (isoflurane and air) for 60 min (4 \times 15 min frames) using a 1.0-mm-diameter pinhole ultra-high sensitivity mouse collimator. One mouse was scanned using a 0.35-mm-diameter pinhole ultra-high resolution mouse collimator. SPECT scans were followed by CT scans (65 kV, 615 μA). SPECT scans were reconstructed with software from MILabs, which uses an ordered-subset expectation maximization algorithm, with a voxel size of 0.375 mm. A 3-dimensional (3D) volume of interest was drawn around the arthritic joints using Inveon Research Workplace software (IAW 4.0; Siemens Preclinical Solutions), and the uptake was quantified as percentage injected dose (%ID). For PET/CT imaging with ^{89}Zr -28H1 and ^{18}F -FDG, mice ($n = 3/\text{group}$) received an intravenous injection of 5–7 MBq of ^{89}Zr -28H1 (injected dose, 50 μg) or 5 MBq of ^{18}F -FDG. For ^{89}Zr -28H1, PET/CT images were acquired with the Inveon animal PET scanner (18) (Siemens Preclinical Solutions) with the mouse under general anesthesia (isoflurane and air) for 20 min at 1 and 3 d after injection. ^{18}F -FDG PET scans (20 min) were acquired 45 min after injection, while mice remained under general anesthesia during the time between injection and imaging. PET scans were followed by CT scans (80 kV, 500 μA). PET scans were reconstructed with Inveon Acquisition Workplace software (version 1.5; Siemens) using an ordered-subset expectation maximization 3D maximum a posteriori algorithm with the following parameters: matrix, 256 \times 256 \times 159; pixel size, 0.43 \times 0.43 \times 0.8 mm; and a uniform-variance maximum a posteriori prior, 0.5 mm. For the biodistribution studies after dissection, mice ($n = 5/\text{group}$) with various macroscopic scores of arthritis received an intravenous injection of 370 kBq of ^{89}Zr -28H1, ^{111}In -28H1, or ^{111}In -DP47GS (injected dose, 50 μg) or 10 MBq of ^{18}F -FDG. At 72 h after injection (^{89}Zr -28H1, ^{111}In -28H1, or ^{111}In -DP47GS) or 1 h after injection (^{18}F -FDG), mice were euthanized by CO_2/O_2 asphyxiation; a blood sample was drawn; and tissues of interest were dissected, weighed, and counted in a γ counter. The %ID per gram of tissue (%ID/g) was calculated for each tissue. Joints were dissected with minimal residual bone or muscle. Uptake in the joints was correlated with the individual arthritis scores of the joints before dissection.

Immunohistochemistry

To demonstrate FAP expression in arthritic murine joints, frozen sections of ankle joints from mice with CIA were stained with monoclonal anti-FAP antibody 28H1 and isotype-matched control DP47GS. Frozen sections of 5 μm were dried overnight at room temperature (RT) and then fixed with ice-cold acetone for 10 min. After drying for at least

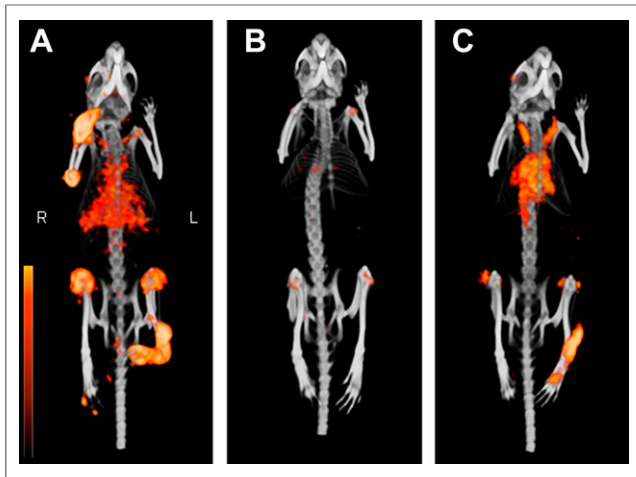


FIGURE 1. 3D SPECT/CT scans of mice with CIA, injected with 15 MBq of ^{111}In -labeled antibody (50 μg). ^{111}In -28H1 at 24 h after injection (A) with joint scores of 1.75, 0, 0.25, and 1.5 (front right, front left, hind right, and hind left, respectively). Radiotracer uptake is clearly visible in inflamed joints. (B) ^{111}In -28H1 at 72 h after injection in healthy mouse. Some bone marrow uptake is visible. (C) ^{111}In -DP47GS at 24 h with joint scores of 0, 0, 2, and 0.5 (front right, front left, hind right, and hind left, respectively). All images are scaled similarly.

1 h at RT, the primary antibody 28H1 or DP47GS was applied and incubated for 1 h at RT. After 3 washing steps with 50 mM PBS, pH 7.4, the secondary antibody goat-antihuman IgG peroxidase was applied. After 30 min at RT, slides were washed 3 times with PBS. Finally, the sections were stained for 10 min with diaminobenzidine and subsequently for 5 s with hematoxylin.

Statistical Analysis

All mean values are mean \pm SD. Unless stated otherwise, statistical analysis was performed using a Welch corrected unpaired Student *t* test or 1-way ANOVA using GraphPad Prism software (version 5.03; Graph-Pad Software). The level of significance was set at a *P* value of less than 0.05.

RESULTS

Immunohistochemistry with 28H1 demonstrated abundant expression of FAP in an inflamed knee joint from a CIA mouse (Supplemental Fig. 1A; supplemental materials are available at <http://jnm.snmjournals.org>). Staining with DP47GS was negative (Supplemental Fig. 1B). Staining with 28H1 on knee tissue from a healthy mouse was also negative (Supplemental Fig. 1C). An *in vitro* binding assay on both human and murine fibroblasts demonstrated high and specific binding to FAP (Supplemental Fig. 2).

SPECT/CT Imaging

To investigate the feasibility of imaging with anti-FAP antibodies in arthritis, CIA was induced in DBA/1J mice, and SPECT/CT and PET/CT imaging with anti-FAP antibody 28H1 were performed after clinical onset of arthritis. ^{111}In -28H1 SPECT/CT scans of mice with arthritic joints clearly demonstrated a strong accumulation of the anti-FAP antibody in the inflamed joints, with little background activity in other tissues. SPECT with ^{111}In -28H1 delineated all inflamed joints, even joints with minimal arthritic scores (0.25 on a scale of 0–2) as well as small, inflamed joints, such as those in the feet and toes. Lungs were also visible on the SPECT scans at 24 h after injection (Fig. 1A), however, this accumulation had disappeared at 72 h after injection (Supplemental Fig. 4A).

The SPECT/CT scan of ^{111}In -28H1 in a healthy mouse at 72 h after injection showed that most of the radioactivity was cleared from the circulation with little bone marrow uptake (Fig. 1B). Whole-body distribution of the isotype-matched control antibody ^{111}In -DP47GS was similar (Fig. 1C), with the exception of a slower clearance from the circulation, resulting in some residual activity in the heart region at 72 h after injection (Supplemental Fig. 4B). With the non-FAP-binding control antibody ^{111}In -DP47GS, the inflamed joints could also be visualized (Fig. 1C), however, to a much lesser extent than with ^{111}In -28H1.

A strong correlation was found between tracer uptake and arthritis severity as demonstrated by quantitative analysis of the SPECT/CT scans at both 1 and 3 d after injection (Fig. 2). Analysis revealed that at both time points the uptake (%ID) correlated well with the arthritis score (at day 1, Spearman's was $\rho = 0.87$ with $P = 0.007$ and at day 3 it was $\rho = 0.89$ with $P = 0.005$). There was good retention of radioactivity in the inflamed joints over the 3-d period. For ^{111}In -DP47GS, no correlation between uptake and arthritis score was found (at day 1, Spearman's was $\rho = 0.51$ with $P = 0.20$ and at day 3 it was $\rho = 0.42$ with $P = 0.30$).

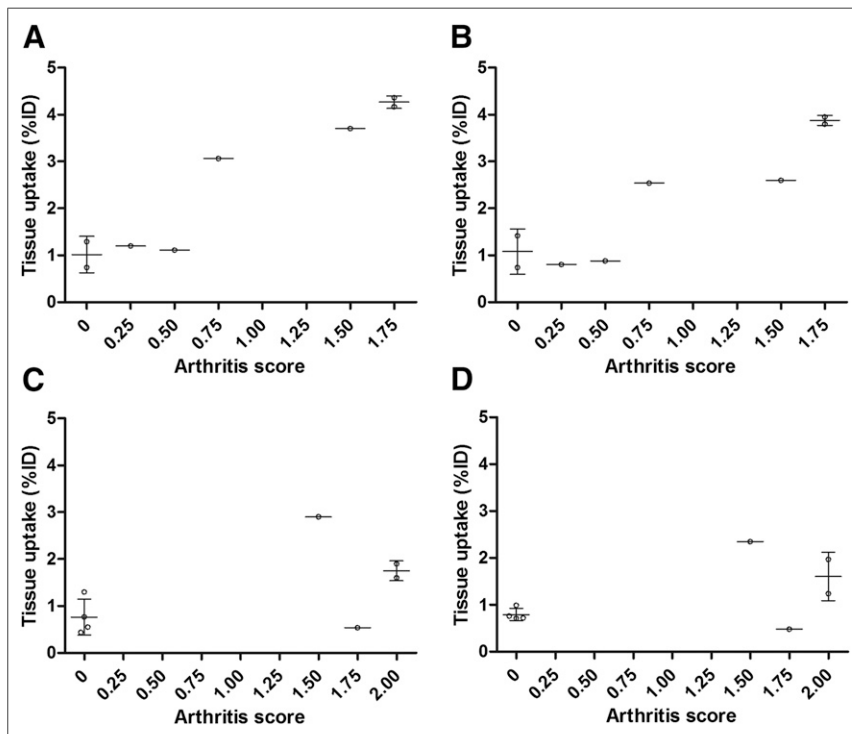


FIGURE 2. Joint uptake vs. score of inflammation based on quantitative analysis of SPECT scans of ^{111}In -28H1 after 1 d (A) and 3 d (B) and of ^{111}In -DP47GS after 1 d (C) and 3 d (D).

PET/CT Imaging

PET/CT images of healthy mice injected with ^{89}Zr -28H1 showed a whole-body distribution similar to the SPECT/CT scans with ^{111}In -labeled 28H1. Excellent targeting of ^{89}Zr -28H1 to inflamed joints was observed, as illustrated by the PET/CT scans (Fig. 3). Healthy mice only displayed accumulation in the heart region and the bone (Supplemental Fig. 5).

PET/CT imaging was also performed with the clinically established radiotracer ^{18}F -FDG, a radiolabeled glucose analog, which accumulates in cells with increased glucose uptake such as tumor cells and inflammatory cells (mainly neutrophils). PET/CT imaging with ^{18}F -FDG showed low uptake in inflamed joints (Fig. 3B). Only severely inflamed joints with a score above 1.25 were visualized, and signal intensity was much lower than that found with the radiolabeled anti-FAP antibodies.

Biodistribution Studies

Biodistribution studies of mice that received ^{111}In -labeled 28H1 revealed that the whole-body distribution of the radioactivity in arthritic mice was similar to that in healthy mice. In line with the quantitative SPECT imaging data, accumulation of ^{111}In -28H1 in the inflamed joints correlated well with the arthritis score as shown in Figure 4A (Spearman ρ , 0.69; $P < 0.0001$). The highest joint uptake of the radiolabeled anti-FAP antibody was found in mice with severely inflamed joints with the maximum arthritis score of 2 (mean, 25.9 ± 4.2 %ID/g; range, 19.0–32.1 %ID/g),

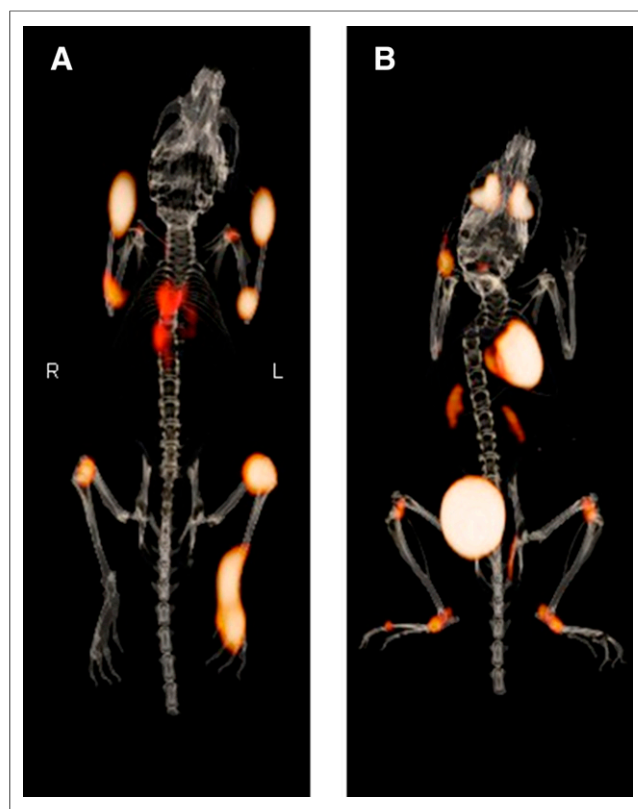


FIGURE 3. (A) PET/CT scans (3D) of mouse with CIA, injected with 5 MBq of ^{89}Zr -28H1 and scanned at 72 h after injection. Joint scores were 1.75, 1.5, 0.25, and 2 (front right, front left, hind right, and hind left, respectively). (B) PET/CT scan of mouse with CIA, injected with 10 MBq of ^{18}F -FDG and scanned at 1 h after injection. Joint scores were 0, 0.25, 1.25, and 0.25 (front right, front left, hind right, and hind left, respectively).

whereas uptake in nonarthritic joints was significantly lower (mean, 4.5 ± 1.1 %ID/g; range, 2.2–6.5 %ID/g; $P < 0.0001$) (Fig. 4A).

Dissection revealed that uptake of ^{111}In -DP47GS in inflamed joints increased only slightly with increasing arthritis scores up to 0.75 but did not increase further in arthritic joints with scores from 0.75 to 2 (Fig. 4B). Uptake of ^{111}In -DP47GS in nonarthritic joints ranged from 1.6 to 8.4 %ID/g (mean, 3.5 ± 1.4 %ID/g). The highest accumulation was found in joints with arthritis scores from 0.75 to 2 but never exceeded 12.0 %ID/g (range, 6.5–12.0 %ID/g; mean, 9.8 ± 1.6 %ID/g). The higher joint uptake of 28H1 than the isotype-matched control antibody DP47GS strongly indicates that the uptake in the arthritic joints was FAP-mediated.

Similar to the ^{111}In -labeled anti-FAP compound, uptake of ^{89}Zr -28H1 in inflamed joints also correlated with the arthritis score (Fig. 4C; Spearman ρ , 0.060; $P < 0.0001$). Joint uptake of ^{89}Zr -28H1 in both normal and inflamed joints was higher than that of ^{111}In -labeled 28H1, possibly partly due to the higher bone uptake of ^{89}Zr than of ^{111}In . The biodistribution study after dissection (72 h after injection) revealed that femoral bone uptake of ^{89}Zr in arthritic mice was significantly higher than that of ^{111}In (32.4 ± 9.2 vs. 5.1 ± 0.4 %ID/g, $P = 0.0016$) (Supplemental Fig. 3).

Interestingly, in mice injected with either ^{111}In -28H1 or ^{89}Zr -28H1, elevated uptake in the bone marrow was observed (Supplemental Fig. 3). ^{111}In -28H1 showed a bone marrow uptake of 8.4 ± 0.9 %ID/g, whereas the uptake of ^{111}In -DP47GS was significantly lower (4.8 ± 1.8 %ID/g, $P = 0.018$), indicating that the bone marrow uptake was also FAP-mediated.

Uptake of ^{18}F -FDG in noninflamed joints was low (mean, 3.3 ± 2.4 %ID/g; range, 1.8–7.5 %ID/g; Fig. 4D), whereas uptake in more severely inflamed joints was higher; joints with scores of 1.75 showed a mean uptake of 6.4 ± 2.6 %ID/g (range, 3.5–10.2 %ID/g) and joints with a score of 2 showed a mean uptake was 9.1 ± 4.5 %ID/g (range, 3.9–11.7 %ID/g).

Localization of the radioactivity in the affected knee joints was demonstrated by a high-resolution scan of an affected knee of a mouse 3 d after injection of ^{111}In -28H1. Figure 5 shows that the radioactivity in the joint is localized in the synovial area of the femur–tibia region and the patella–femur region.

DISCUSSION

With SPECT and PET imaging, we demonstrated that radiolabeled anti-FAP antibodies specifically targeted to inflamed joints in an experimental model of RA. In addition, the present study showed that the uptake of the radiolabeled antibody correlated with the arthritis severity.

Until now, targeting of FAP with radiolabeled antibodies has been studied exclusively in tumor models because FAP is abundantly expressed on carcinoma-associated fibroblasts in the tumor stroma. Good and specific targeting of tumors with ^{131}I -labeled murine F19 (9) and ^{131}I -labeled sibtrotuzumab, a humanized version of the F19 antibody (10), has been demonstrated. However, because of the lack of therapeutic effect and the occurrence of human–antihuman antibodies, further clinical development of sibtrotuzumab was halted. Engineering human Fab fragments into fully human IgG1 led to the development of 2 anti-FAP antibodies, ESC11 and ESC14. These rapidly internalizing, ^{177}Lu -labeled antibodies showed good tumor targeting and a significant therapeutic effect in melanoma-xenografted mice (11).

Besides expression in tumor stroma and granulation tissue of healing wounds (4), FAP is also abundantly expressed by fibroblast-like synoviocytes in RA (2). It was also shown that the expression

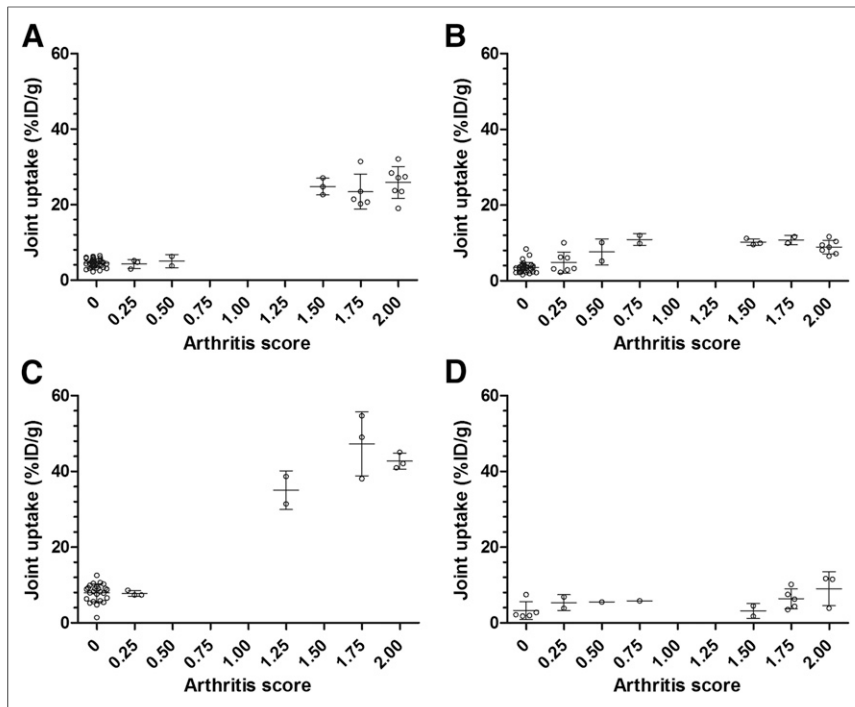


FIGURE 4. Joint uptake vs. macroscopic score of arthritis of ^{111}In -28H1 (A), ^{111}In -DP47GS (B), ^{89}Zr -28H1 (C), and ^{18}F -FDG (D). Joint uptake was measured in dissected tissues, 3 d after injection of radiolabeled antibodies.

of FAP was higher in RA than in osteoarthritis. The authors speculated that the pronounced expression of FAP in RA might be related to the degree of synovial inflammation. Analyzing the gene expression profiles in inflamed paws of CIA mice confirmed that FAP expression was 7-fold increased in inflamed paws as compared with noninflamed paws (19). Therefore, we hypothesized that imaging of

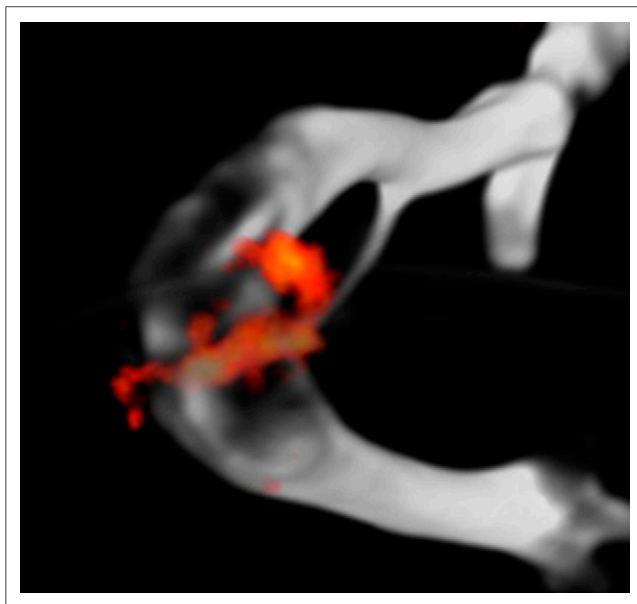


FIGURE 5. High-resolution 3D SPECT/CT scan of knee joint (score, 0.75) of arthritic DBA/1J mouse intravenously injected with ^{111}In -28H1 and scanned at 72 h after injection. Radioactivity was mainly localized to synovial area of femur-tibia and patella-femur regions.

FAP expression with 28H1 might be a valuable tool to assess the severity of the inflammation. Here, we demonstrated that the uptake of the anti-FAP antibody 28H1 increased with enhanced severity of inflammation. It is therefore anticipated that anti-FAP imaging might be a new sensitive tool for scoring RA disease activity and could possibly be of additive value to existing scoring systems such as DAS28. Most importantly, it might allow noninvasive early therapy response monitoring.

The nonspecific isotype-matched control antibody DP47GS also localized in inflamed joints, but the accumulation did not increase with increasing severity at higher scores, leading us to conclude that the major part of the uptake of 28H1 in inflamed joints was FAP-mediated. Enhanced uptake of DP47GS in inflamed joints was due to locally enhanced vascular permeability at inflamed sites, resulting in extravasation of larger molecules such as antibodies, also known as the enhanced permeability and retention effect (20). This effect has been shown with $^{99\text{m}}\text{Tc}$ -labeled nonspecific polyclonal IgG in a rat model of arthritis (21).

In the present study, imaging was performed with both ^{89}Zr - and ^{111}In -labeled FAP antibody 28H1. Although the image

quality was similar for both radionuclides, ^{89}Zr -28H1 had the disadvantage of enhanced uptake in the bone, most likely caused by unbound ^{89}Zr , released from the radiolabeled antibody after metabolism *in vivo*. This phenomenon has been described in previous studies with ^{89}Zr -anti-EGFR and anti-IGF1R antibodies (22,23). Also others reported elevated bone uptake of ^{89}Zr , compared with ^{111}In (23,24). When imaging inflamed joints and bone-related disorders, this elevated bone uptake is unwanted and hampers the interpretation of the scans. Therefore, the use of ^{111}In for imaging with anti-FAP antibodies in RA is preferred over that of ^{89}Zr .

Radionuclide imaging in RA has been mainly focused on ^{18}F -FDG PET/CT imaging (25), but also radiolabeled peptides such as IL1- α , annexin-V, and small molecules such as folate, PK11195, and matrix metalloproteinase- and E-selectin-targeting molecules have been investigated both clinically or preclinically (26). In addition, radiolabeled antibodies such as anti-CD20 (rituximab) and anti-TNF α (infliximab) have been studied. Although these tracers accumulated specifically in affected joints, uptake could generally not be correlated with the severity of the inflammation. ^{18}F -FDG has been studied extensively, and joint accumulation has been proven to correlate with disease activity scores (27,28), and we therefore also included ^{18}F -FDG in our studies as a reference. However, uptake of ^{18}F -FDG in arthritic joints in the CIA model was relatively low and did not correlate with the severity of the inflammation, which is in line with previous preclinical studies (29,30), although 1 study reported a good correlation (31). These differences might be explained by the use of various models, but also imaging might have been performed at various time points after the onset of the arthritis. Therefore, ^{18}F -FDG PET imaging of experimental arthritis in mice is considered to be of limited value. Generally, neutrophils and activated macrophages mainly contribute

to ¹⁸F-FDG uptake in inflammatory diseases. However, in rats with CIA it was shown that increased accumulation was mainly caused by uptake in activated fibroblasts in the pannus, rather than by neutrophils (32).

We noted an unexpectedly high bone marrow uptake of the 28H1 anti-FAP antibody, which was not observed with the isotype-matched control antibody DP47GS. This low uptake of the control antibody indicates that the uptake of 28H1 was specific and most likely FAP-mediated. These findings corroborate a recent study in which it has been described that both mouse and human pluripotent bone marrow stem cells could be recognized by FAP-reactive T cells (33).

CONCLUSION

SPECT/CT imaging with the anti-FAP antibody ¹¹¹In-28H1 specifically visualized arthritic joints with high resolution, and accumulation correlated with the severity of the inflammation in murine experimental arthritis. Background uptake of the radiolabeled antibody was low, resulting in excellent image quality. Future studies will focus on the potential role of 28H1 as a tool to monitor therapy response early after the start of treatment.

DISCLOSURE

The costs of publication of this article were defrayed in part by the payment of page charges. Therefore, and solely to indicate this fact, this article is hereby marked "advertisement" in accordance with 18 USC section 1734. This study was funded in part by the Roche Postdoc Fellowship (RPF) Program. No other potential conflict of interest relevant to this article was reported.

ACKNOWLEDGMENT

We thank Anniek van der Waart, PhD, Department of Laboratory Medicine, Laboratory of Hematology, Radboud University Medical Center, Nijmegen, The Netherlands, for expert help in the analysis of bone marrow samples.

REFERENCES

1. Firestein GS. Invasive fibroblast-like synoviocytes in rheumatoid arthritis: passive responders or transformed aggressors? *Arthritis Rheum.* 1996;39:1781–1790.
2. Bauer S, Jendro MC, Wadle A, et al. Fibroblast activation protein is expressed by rheumatoid myofibroblast-like synoviocytes. *Arthritis Res Ther.* 2006;8:R171.
3. Scanlan MJ, Raj BK, Calvo B, et al. Molecular cloning of fibroblast activation protein alpha, a member of the serine protease family selectively expressed in stromal fibroblasts of epithelial cancers. *Proc Natl Acad Sci USA.* 1994;91:5657–5661.
4. Grinnell F. Fibroblasts, myofibroblasts, and wound contraction. *J Cell Biol.* 1994;124:401–404.
5. Morimoto C, Schlossman SF. The structure and function of CD26 in the T-cell immune response. *Immunol Rev.* 1998;161:55–70.
6. Goldstein LA, Ghersi G, Pineiro-Sanchez ML, et al. Molecular cloning of serpinase: a serine integral membrane protease from human melanoma. *Biochim Biophys Acta.* 1997;1361:11–19.
7. Garin-Chesa P, Old LJ, Rettig WJ. Cell surface glycoprotein of reactive stromal fibroblasts as a potential antibody target in human epithelial cancers. *Proc Natl Acad Sci USA.* 1990;87:7235–7239.
8. Park JE, Lenter MC, Zimmermann RN, Garin-Chesa P, Old LJ, Rettig WJ. Fibroblast activation protein, a dual specificity serine protease expressed in reactive human tumor stromal fibroblasts. *J Biol Chem.* 1999;274:36505–36512.
9. Welt S, Divgi CR, Scott AM, et al. Antibody targeting in metastatic colon cancer: a phase I study of monoclonal antibody F19 against a cell-surface protein of reactive tumor stromal fibroblasts. *J Clin Oncol.* 1994;12:1193–1203.

10. Scott AM, Wiseman G, Welt S, et al. A phase I dose-escalation study of sibtuzumab in patients with advanced or metastatic fibroblast activation protein-positive cancer. *Clin Cancer Res.* 2003;9:1639–1647.
11. Fischer E, Chaitanya K, Wuest T, et al. Radioimmunotherapy of fibroblast activation protein positive tumors by rapidly internalizing antibodies. *Clin Cancer Res.* 2012;18:6208–6218.
12. Bacac M, Freimoser-Grundschober A, Hosse R, et al., inventors; Roche Glycart, assignee. Anti-FAP Antibodies and Methods of Use. U.S. patent WO/2012/020006. February 16, 2012.
13. Baehner M, Jenewein S, Kubbies M, Moessner E, Schlothauer T; Roche Glycart, assignee. Antibody Fc variants. U.S. patent WO/2012/130831. October 4, 2013.
14. Brom M, Joosten L, Oyen WJ, Gotthardt M, Boerman OC. Improved labelling of DTPA- and DOTA-conjugated peptides and antibodies with ¹¹¹In in HEPES and MES buffer. *EJNMMI Res.* 2012;2:4.
15. Verel I, Visser GW, Boellaard R, Stigter-van Walsum M, Snow GB, van Dongen GA. ⁸⁹Zr immuno-PET: comprehensive procedures for the production of ⁸⁹Zr-labeled monoclonal antibodies. *J Nucl Med.* 2003;44:1271–1281.
16. Joosten LA, Helsen MM, van de Loo FA, van den Berg WB. Anticytokine treatment of established type II collagen-induced arthritis in DBA/1 mice: a comparative study using anti-TNF alpha, anti-IL-1 alpha/beta, and IL-1Ra. *Arthritis Rheum.* 1996;39:797–809.
17. van der Have F, Vastenhouw B, Ramakers RM, et al. U-SPECT-II: an ultra-high-resolution device for molecular small-animal imaging. *J Nucl Med.* 2009;50:599–605.
18. Visser EP, Disselhorst JA, Brom M, et al. Spatial resolution and sensitivity of the Inveon small-animal PET scanner. *J Nucl Med.* 2009;50:139–147.
19. Ibrahim SM, Koczan D, Thiesen HJ. Gene-expression profile of collagen-induced arthritis. *J Autoimmun.* 2002;18:159–167.
20. Maeda H, Seymour LW, Miyamoto Y. Conjugates of anticancer agents and polymers: advantages of macromolecular therapeutics in vivo. *Bioconjug Chem.* 1992;3:351–362.
21. Boerman OC, Oyen WJ, Storm G, et al. Technetium-99m labelled liposomes to image experimental arthritis. *Ann Rheum Dis.* 1997;56:369–373.
22. Heskamp S, van Laarhoven HW, Molkenboer-Kuonen JD, et al. ImmunoSPECT and immunoPET of IGF-1R expression with the radiolabeled antibody R1507 in a triple-negative breast cancer model. *J Nucl Med.* 2010;51:1565–1572.
23. Perk LR, Visser GW, Vosjan MJ, et al. ⁸⁹Zr as a PET surrogate radioisotope for scouting biodistribution of the therapeutic radiometals ⁹⁰Y and ¹⁷⁷Lu in tumor-bearing nude mice after coupling to the internalizing antibody cetuximab. *J Nucl Med.* 2005;46:1898–1906.
24. Dijkers EC, Kosterink JG, Rademaker AP, et al. Development and characterization of clinical-grade ⁸⁹Zr-trastuzumab for HER2/neu immunoPET imaging. *J Nucl Med.* 2009;50:974–981.
25. Kubota K, Ito K, Morooka M, et al. FDG PET for rheumatoid arthritis: basic considerations and whole-body PET/CT. *Ann N Y Acad Sci.* 2011;1228:29–38.
26. Mountz JM, Alavi A, Mountz JD. Emerging optical and nuclear medicine imaging methods in rheumatoid arthritis. *Nat Rev Rheumatol.* 2012;8:719–728.
27. van der Laken CJ, Huisman MH, Voskuyl AE. Nuclear imaging of rheumatic diseases. *Best Pract Res Clin Rheumatol.* 2012;26:787–804.
28. Roivainen A, Hautaniemi S, Mottonen T, et al. Correlation of ¹⁸F-FDG PET/CT assessments with disease activity and markers of inflammation in patients with early rheumatoid arthritis following the initiation of combination therapy with triple oral antirheumatic drugs. *Eur J Nucl Med Mol Imaging.* 2013;40:403–410.
29. Irmiler IM, Opfermann T, Gebhardt P, et al. In vivo molecular imaging of experimental joint inflammation by combined ¹⁸F-FDG positron emission tomography and computed tomography. *Arthritis Res Ther.* 2010;12:R203.
30. Cha JH, Lee SH, Lee SW, et al. Assessment of collagen-induced arthritis using cyanine 5.5 conjugated with hydrophobically modified glycol chitosan nanoparticles: correlation with ¹⁸F-fluorodeoxyglucose positron emission tomography data. *Korean J Radiol.* 2012;13:450–457.
31. Kundu-Raychaudhuri S, Mitra A, Datta-Mitra A, Chaudhari AJ, Raychaudhuri SP. In vivo quantification of mouse autoimmune arthritis by PET/CT. *Int J Rheum Dis.* June 26, 2014 [Epub ahead of print].
32. Matsui T, Nakata N, Nagai S, et al. Inflammatory cytokines and hypoxia contribute to ¹⁸F-FDG uptake by cells involved in pannus formation in rheumatoid arthritis. *J Nucl Med.* 2009;50:920–926.
33. Tran E, Chinnasamy D, Yu Z, et al. Immune targeting of fibroblast activation protein triggers recognition of multipotent bone marrow stromal cells and cachexia. *J Exp Med.* 2013;210:1125–1135.